UC Berkeley

Title

Concentration Dependence of Dopant Electronic Structure in Bottom-up Graphene Nanoribbons

Permalink

https://escholarship.org/uc/item/0gd8d3c8

Journal

Nano Letters, 18(6)

ISSN

1530-6984

Authors

Pedramrazi, Zahra
Chen, Chen
Zhao, Fangzhou
et al.

Publication Date

2018-06-13

DOI

10.1021/acs.nanolett.8b00651

Peer reviewed

Concentration dependence of dopant electronic structure in bottom-up graphene nanoribbons

Zahra Pedramrazi[1†], Chen Chen[2,3†], Fangzhou Zhao[1†], Ting Cao[1,3], Giang D. Nguyen[1], Arash A. Omrani[1], Hsin-Zon Tsai[1], Ryan R. Cloke[2], Tomas Marangoni[2], Daniel J. Rizzo[1], Trinity Joshi[1], Christopher Bronner[1], Won-Woo Choi[1], Felix R. Fischer[2,3,4*], Steven G. Louie[1,3*], Michael F. Crommie[1,3,4*]

1 Department of Physics, University of California at Berkeley, Berkeley, California 94720, USA. 2 Department of Chemistry, University of California at Berkeley, Berkeley, California 94720, USA. 3 Materials Sciences Division, Lawrence Berkeley National Laboratory, Berkeley, California 94720, USA. 4 Kavli Energy NanoSciences Institute at the University of California and Lawrence Berkeley National Laboratory, Berkeley, California 94720, USA. †These authors contributed equally to this work. *e-mail: ffischer@berkeley.edu; sglouie@berkeley.edu; crommie@berkeley.edu

Abstract

Bottom-up fabrication techniques enable the atomically precise integration of dopant atoms into the structure of graphene nanoribbons (GNRs). As such, the dopants are systematically aligned in GNRs, behaving distinctly from those in bulk semiconductors. However, the effect of dopant concentration on electronic structures of GNRs remains unknown, despite its importance in future electronic applications. Here we use scanning tunneling microscopy and first-principles calculations to investigate the electronic structure of bottom-up synthesized N=7 armchair GNRs featuring varying concentrations of boron dopants. First-principles calculations of freestanding GNRs predict that the inclusion of boron atoms into GNRs' backbone should induce two sharp dopant states whose energy splitting varies with the dopant concentration. Scanning tunneling spectroscopy experiments, however, reveal two broad dopant states with an energy splitting greater than expected. This anomalous behavior results from heretofore unrecognized hybridization between the dopant states and the Au (111) surface, having interaction strength dictated by dopant-orbital symmetry.

Introduction

Quasi-one-dimensional graphene nanoribbons (GNRs) hold promise as a new platform for future nanoelectronics applications[1-9]. Analogous to traditional semiconductors, their electronic structure can be tailored by the introduction of heteroatom impurities[10-14]. The effect of impurity doping on GNRs, however, is not easily understood using the common framework of traditional semiconductor materials[15, 16]. GNRs, for example, are intrinsically in the regime of strong quantum confinement and exhibit trigonal planar symmetry rather than the more common tetrahedral symmetry, leading to conduction through extended π-networks unlike conventional semiconducting systems. Bottom-up synthesis has provided an effective method to explore heteroatom doping in GNRs since it enables site-specific incorporation of heteroatom dopants through the design of functional precursor molecules that can be assembled into atomically-precise doped GNRs[4, 17-22]. The introduction of nitrogen atoms into GNR edges, for example, has been shown to shift the energy-level alignment of the GNR band structure[10, 11], while the incorporation of boron atoms into the GNR backbone has been shown to introduce new in-gap states[23-25]. The electronic structure of boron-induced dopant states, including the effects of substrate hybridization, remains poorly understood[21-25].

Here we report the bottom-up synthesis and characterization of boron-doped N=7 armchair GNRs (AGNR) at two antipodal doping regimes: the dilute and highly dense limits. Scanning tunneling spectroscopy (STS) measurements and density functional theory (DFT) calculations were performed to study the local electronic properties of boron-doped GNRs in both concentration regimes. The calculations were further validated with GW calculations[26] for the freestanding case. Our calculations show that there exist two boron-induced dopant states in the gap having one with s-like (even parity) and the other with p-like (odd parity) orbital character

2

that persist in both concentration limits. In the dilute limit our freestanding calculations (i.e., no substrate coupling) show that the boron-induced dopant states are nearly degenerate. As the density of dopant atoms increases in the freestanding regime the energy separation between the boron-induced states increases and the dopant states form impurity bands since the dopants are arranged periodically. Our experiments, on the other hand, are not consistent with the predicted results of the freestanding GNR. In the dilute limit, we observe two dopant states with different symmetries, strongly split in energy and broadened into asymmetric peaks (i.e., one is broader than the other). In the dense limit the experimental upper dopant energy band is shifted in energy with respect to the theoretical prediction and is significantly broader than expected. This anomalous behavior is explained by hybridization between the boron-induced dopant states and the surface state of the gold substrate. First-principles calculations, taking substrate coupling into account, confirm that there is a strong and symmetry-dependent hybridization between GNR dopant states and Au (111), which induces strong energy splitting and asymmetrical broadening whose magnitude depends on the dopant state symmetry.

Results

Fig. 1 shows the calculated DFT with local density approximation (LDA)electronic structure of a freestanding (i.e., no substrate included in the calculation) N=7 AGNR for three boron dopant concentrations: (i) the undoped case (Fig. 1d), (ii) the dilute doping limit (Fig. 1e), and (iii) the dense doping limit (Fig.1f) (Figs. 1a-c show the unit cells used for all three calculations). GW[26] calculations give similar results but with larger bandgap values due to self-energy effects. We focus on the DFT results here since nonlocal substrate screening in general will reduced the GW gaps to close to the DFT level when the system is put on a metallic surface. The undoped GNR band structure shows the familiar conduction (CB) and valence (VB) bands

that have been calculated within DFT before[26], and the dilute-doped GNR exhibits band edges at similar energies. The most significant difference between the undoped and dilute-doped band structure is the presence of two new defect levels at ~0.5 eV above the VB edge for the latter case (the appearance of new bands above (below) the conduction (valence) band edge for the dilute limit is due to band-folding effects from the supercell geometry in the calculation). The new impurity states are nearly degenerate with a splitting < 20 meV and exhibit large contribution from the π-orbitals of the boron dopant atoms. Analysis of the wavefunction for the lower defect state shows that it has *p*-like (odd parity) symmetry along the GNR axial direction (Fig. S1(b) in the Supplementary Information (SI)), while the upper defect state has *s*-like symmetry (even parity) along the longitudinal axis (Fig. S1(c)) (a similar theoretical result for the dilute, freestanding limit was reported in ref.25). As the dopant concentration increases, the energy splitting between the two impurity states correspondingly increases and the defect states evolve into impurity bands with an energy gap of 0.5 eV, as shown in the band structure plot for the densely-doped GNR in Fig.1f (Fig. S2 in the SI shows the band structures for other intermediate dopant densities).The symmetry of the dopant bands changes as a function of crystal momentum due to an anti-crossing that causes two otherwise dispersive bands of pure symmetry character to hybridize into a pair of flat bands of width< 0.12 eV in the densely-doped limit.

In order to experimentally test these unusual theoretical predictions, GNRs were fabricated in the dilute-doped regime by combining molecular precursors for undoped N=7 GNR (10,10'-dibromo-9,9'-bianthryl, DBBA) with precursors for boron-doped N=7 AGNR (Fig. S3) in a 10:1 ratio (undoped: boron-doped) using standard GNR growth conditions[4, 18, 19](polymerization of the precursors occurs at ~180 °C while cyclodehydrogenation occurs at ~360 °C(see methods)).

Fig. 2b shows an STM topographic image of a resulting dilute-doped N=7 GNR on Au (111) with vertical dashed lines indicating the location of a boron defect (a sketch of the wireframe structure is shown in Fig. 2a). The region surrounding the dopant atoms has a reduced apparent height in the STM image, suggesting that the boron atoms sit closer to the Au (111) surface than the GNR carbon atoms.

The electronic structure of dilute-doped GNRs was investigated by measuring STM differential conductance (dI/dV) spectra at the position of boron dopants and then comparing the acquired spectra to those of undoped GNR segments at the positions marked in Fig. 2b (the respective positions are color-coded with the dI/dV curves). Fig. 2c shows a characteristic dI/dV point spectrum (green curve) recorded at the edge of an undoped segment of the GNR. This spectrum exhibits a peak at V_s = 1.68 ± 0.02V, which we identify as the CB edge, as well as a peak at V_s = −0.80 ± 0.02 V identified as the VB edge (V_s is sample voltage). This leads to an overall GNR bandgap of 2.48 ± 0.02 eV, similar to bandgap measurements on undoped N=7 AGNR performed previously[27-29]. The identity of these familiar spectroscopic peaks was confirmed via energy-resolved dI/dV mapping, which allows visualization of the surface local density of states (LDOS) depicted in Figs. 2d–g. Two new states (see insets to Fig. 2c) attributed to the dopant atoms are be observed in STM spectroscopy measured at the center (top inset, blue curve) and edge (bottom inset, red curve) of the boron defect shown in Fig. 2b. The dI/dV spectrum measured at the impurity edge shows the presence of a new peak (State 1) that is centered at V_s = −0.52 ± 0.02 V (280mV higher in energy than the VB edge) and has a full width at half maximum (FWHM) of 0.23V. The dI/dV spectrum measured at the position of the dopant atoms exhibits a pronounced upward slope starting at V_s = ~0.3 V and extending to V_s = ~1.2 V that is not observed in the reference spectrum taken at the center of the undoped segment with

5

the same tip (top inset, black curve). We label this dopant-induced feature (which was reproducibly observed in different GNRs with different tips) as State 2.

The spatial distribution of these two-new dopant-induced spectroscopic features (State 1 and State 2) was determined using dI/dV mapping. Fig. 2f shows a dI/dV map measured at the energy of State 1 that exhibits bright lines along the edges of the dopant segment as well as two small high intensity spots near the boron atoms (the two central hot-spots are located at the sites of the two horizontal boron-carbon bonds in Fig. 2a). Fig. 2e shows a representative dI/dV map of State 2recordedat 0.8V that exhibits an elliptical, bright but diffuse LDOS centered at the position of boron atoms (dI/dV maps recorded for State 2 over the energy range 0.3 V $< V_s <$1.3 V show similar LDOS patterns, see SI Fig. S4).

We next explored GNRs doping with boron atoms in the dense limit. These GNRs were grown using exclusively the boron-doped precursor (Fig. S3b). A schematic representation of the resulting boron-doped GNR structure is depicted in Fig. 3b, along with an STM topograph in the inset of Fig. 3a. As shown previously for this type of GNR[23, 24],the boron-doped segments of the GNR sit slightly closer to the substrate than the unsubstituted regions and lead to a 1.30 ±0.05 nm periodic height modulation along the GNR long axis in the topography. We initially explored the electronic structure of densely-doped GNRs via dI/dV point spectroscopy. Fig. 3a shows typical dI/dV spectra measured at a position along the backbone (blue curve) and at the edge (red curve) of a densely-doped GNR with the same tip. The dI/dV spectrum recorded at the GNR edge shows a well-defined peak at 1.63 ± 0.04 eV above E_F[24]. The spectrum recorded along the densely-doped GNR backbone appears quite different and reveals a new broad spectroscopic feature at 1.0 ± 0.2 eV above E_F (this peak is absent in STS of undoped GNRs[27, 29, 30]). We were

6

unable to observe any reproducible spectroscopic features below E_F in our dI/dV point spectra recorded for densely-doped GNRs on Au (111).

We used dI/dV mapping to visualize the electronic structure of densely-doped GNRs at different energies. Fig. 3c shows a dI/dV map recorded at +1.60 eV, the energy of the upper spectroscopic peak. Here intensity of the LDOS is highest along the GNR edges, similar to what has previously been observed for energies near the CB edge in undoped N=7 AGNRs[24, 27-29].The dI/dV map obtained at an energy near the broader spectroscopic peak (+1.00 eV) shows a pronounced shift in LDOS from the GNR edges to the GNR backbone (Fig. 3d).Fig. 3e shows the dI/dV map obtained at a voltage of V_s = –0.23 V. Although we observe no reproducible peak-like feature at this energy in the dI/dV point spectroscopy, a clear transition is observed in the spatial LDOS distribution between the dI/dV map measured at this energy and maps obtained at higher voltages (see Fig. S6 in the SI). The dI/dV map at V_s = –0.23 V, for example, transfers LDOS outward to the GNR edges and features a nodal structure compared to the map at V_s = +1.00 V. The spatial distribution of the states observed at V_s = 1.00 V and V_s = –0.23 V are quite different from what is observed in the case of undoped N=7 GNRs, and so the differences must arise from the influence of the boron dopants.

While some of our experimental results for dilute and densely-doped GNRs are qualitatively in agreement with our theoretical calculations for freestanding boron-doped GNRs, significant discrepancies remain. In the dilute-doping limit our experiments faithfully reproduce the two expected defect states in the gap with one exhibiting s-like symmetry (State 2, which has no node) and the other exhibiting p-like symmetry (State 1, which has a node). While the theoretical defect states are essentially degenerate, experimental measurements show a significant splitting between the two states (~ 1 eV). Furthermore, it is not clear why the

experimental feature seen for State 1 is so much narrower than the broad, sloping spectroscopic feature that defines State 2.

In the densely-doped regime, the peak observed at $V_s = 1.6$ eV (Fig.3a, red curve) is consistent with the theoretically predicted CB (Fig. 1f). The new spectroscopic peak at $V_s = +1.0$ V that spatially localizes along the GNR backbone(Fig. 3a, blue curve) also roughly corresponds to spectroscopic features expected to arise from a new dopant-induced band[25](e.g., the upper dopant band in Fig. 1f). However, there remain a number of discrepancies between experiment and theory in the densely-doped regime. Most significant is the energy alignment of the observed spectroscopic features. The energy difference between the two experimental spectroscopic peaks shown in Fig. 3a is only ~0.5 eV whereas the theoretically predicted energy difference between the CB and the upper dopant band in Fig.1f is ~1.5 eV. Also, if the state imaged at $V = -0.23$ eV (Fig.3e) is assigned to the lower dopant band then the energy difference between the two dopant-induced bands in the experiment (~1.2eV) is significantly larger than the calculated energy difference (0.5eV). Moreover, the anomalously broad spectroscopic peak at $V_s = +1.0$ V is inconsistent with the simulation since the upper dopant bandwidth is predicted to be quite narrow (Fig. 1f).

We conclude that a freestanding GNR model used in the calculations is insufficient to describe our experimental data, most likely because it neglects the substrate. Therefore, in order to better understand our experimental results, we performed additional calculations that take into account the underlying Au (111) substrate upon which the boron-doped GNRs rest. The electronic structure of dilute-doped GNRs including the Au (111) substrate was calculated via DFT using the supercell shown in Fig. 4d. Similar to our experimental data, the boron atoms in a fully-relaxed simulated GNR sit closer to the Au (111) surface than the carbon atoms in undoped

segments of the ribbon. This reduction of the boron-gold distance indicates significant interaction between the boron dopants and the gold substrate atoms.

In order to simulate the dilute-doped dI/dV spectroscopy of Fig. 2c, we calculated the energy-resolved charge density (*including* the gold substrate effects) averaged over a 7.5 Å × 7.5 Åarea located 3 Å above the boron-doped segment that follows the topography of the GNR. The results are depicted in the plot of Fig. 4a. Significant in-gap features appear in the otherwise gapped region due to the hybridization between the GNR states with the underlying Au (111) substrate states. In particular, two broad features are observed that arise from the boron defect, one occupied and the other one unoccupied. The occupied feature appears in the range –0.4 eV <E< –0.1 eV and exhibits the LDOS pattern shown in Fig. 4c (obtained at E = –0.21 eV). (Fig. 4f shows the real part of the wavefunction of the state at E = –0.21 eV, plotted along the dashed line in Fig.4c). This locally-averaged LDOS has bright features at the outer edges and exhibits two interior peaks of high intensity. The wavefunction of that state has odd parity (*p*-like) under mirror symmetry. Comparing with the occupied feature, the unoccupied one is quite different: a much broader feature arises over the range 0.3 eV <E< 0.9 eV and has a slight dip at E ~ 0.5 eV. Fig.4b shows a representative LDOS map of this defect state (obtained at E = 0.38 eV) and Fig. 4e shows a line cut of the corresponding wavefunction at this energy. This defect state is more delocalized than the occupied state and the wavefunction shows approximate even parity (*s*-like).

The theoretical CB and VB edges for this system were determined by examining the undoped segment of the dilute doped GNR on gold (here undoped indicates the segment that does not directly include any boron atoms, see Fig. S5 in the SI). This allowed us to resolve a conduction band edge at approximately E = 1.6 eV, as well as evidence for the valence band

edge near $E = -0.9$ eV. This identification was confirmed by calculating LDOS maps at these energies (Fig. S5).

The simulated behavior of the dilute-doped GNR on Au (111) supports our hypothesis that the differences observed between the experiment and the "freestanding" theory arise from the interaction between the boron-doped GNRs and the gold substrate. Due to the reasonably good agreement in the energy positions and broadening of the defect states, we identify the occupied and unoccupied features in the calculation with experimentally observed State 1 and State 2, respectively. Further evidence for this assignment can be found in the simulated LDOS patterns. For example, the theoretical LDOS pattern for the occupied state feature (Fig. 4c) looks strikingly similar to State 1, while the bright, delocalized unoccupied state feature (Fig. 4b) resembles State 2. The energy splitting between the simulated central energy of the two peaks (~1 V) is also similar to what is observed experimentally, indicating that the boron-induced defect states (which are nearly degenerate for a freestanding GNR) are split by interaction with the Au (111) substrate. This interaction leads to significant and different broadening for the two defect states, which is faithfully reproduced by the calculation. The symmetry of the calculated defect state wavefunctions offers an explanation for the difference in broadening observed for the two states since State 1 has p-like character which should hybridize more weakly with the s-like surface states of gold (due to the phase difference in the two lobes of the p-like wavefunction), whereas State 2 has s-like character and so is expected to hybridize more strongly with gold. The s- and p-like symmetry of the boron defect states is thus a primary factor in determining the dopant electronic structure for the strongly hybridized boron-doped GNR/Au (111) complex.

The agreement between experiment and theory for dilute-doped GNRs in the presence of coupling to Au (111) also helps us to better understand GNR behavior in the densely-doped regime. The freestanding GNR model in this regime (Fig. 1f) predicts a larger energy difference between the CB edge and upper dopant band and a narrower dopant band width than observed in the experimental. However, if strong coupling to the Au (111) surface is considered, then the experimental observations in the densely-doped regime can be rationalized. The increase in the energy of the upper dopant band, for example, is a result of the interaction with the Au (111) surface (similar to the splitting of the dilute doping states). The large broadening of the upper dopant band is rationalized by the particularly strong coupling that exists between the *s*-like dopant state and the gold substrate, since the upper and lower dopant state are always *s*-like and *p*-like, respectively, independent of concentrations for randomly distributed boron pairs or at the zone center for periodical distributed pairs. This is further supported by the fact that the experimental d*I*/d*V* map of the upper dopant band states (Fig. 3d) resembles a superposition of *s*-like State 2 density maps while the d*I*/d*V* map of the lower defect band states (Fig.3e) more resembles a superposition of *p*-like State 1 density maps.

Hybridization of the dopant atoms with the underlying Au (111) substrate has an unusually strong impact on the electronic structure of boron-doped GNRs. *s*-like dopant states hybridize more efficiently with gold than *p*-like defect states due to their symmetry, while both types of dopant states are broadened and the two split in energy. We expect very a different electronic behavior for boron-doped GNRs placed on substrates that interact less strongly with boron impurity atoms than gold.

METHODS

All STM and STS measurements were performed at T = ~7 K. Molecular precursors for bottom-up synthesized GNRs were deposited onto a clean Au (111) single crystal surfaces held at 24 °C (both types simultaneously in the case of the dilute-doped GNRs). The sample was then gradually annealed to 640 K over 30 minutes and held at that temperature for 40 min to induce the polymerization and cyclodehydrogenation necessary to form boron-doped GNRs. The spectroscopic features reported here (including dI/dV maps) were consistently observed on thirteen different dilute-doped GNRs and eleven different densely-doped GNRs whose electronic properties were inspected using a variety of different STM tips. All STM topographic images were processed using WSxM[31].

First-principles calculations were performed using DFT in the local density approximation, implemented in the Quantum Espresso[32] package. We used ultrasoft pseudopotentials with a plane-wave energy cutoff of 40 Ry to calculate freestanding boron-doped GNRs as well as boron-doped GNRs on Au (111). Dangling bonds were capped by hydrogen and all structures were fully relaxed until the force on each atom was less than 0.02 eV Å^{-1}. For calculations that included a gold substrate the GNR was positioned on top of Au (111) surface that included 288 gold atoms in 4 layers within the supercell. The GNR was placed perpendicular to the Au(110)crystallographic direction to ensure commensuration between the unit cell of gold and the GNR to within less than 1% lattice mismatch. The GNR was slightly strained initially to fit the lattice constant of gold, but was then fully relaxed until the forces on every atom were less than 0.02 eV Å^{-1}. GW calculations were performed using the BerkeleyGW package[33].

REFERENCES

1.   Shen, Y.-T. et al. Switchable Ternary Nanoporous Supramolecular Network on Photo-Regulation. *Nano Letters* **11**, 3245-3250 (2011).
2.   Son, Y.-W., Cohen, M.L. & Louie, S.G. Half-metallic graphene nanoribbons. *Nature* **444**, 347-349 (2006).
3.   Bennett, P.B. et al. Bottom-up graphene nanoribbon field-effect transistors. *Applied Physics Letters* **103**, 253114 (2013).
4.   Cai, J. et al. Atomically precise bottom-up fabrication of graphene nanoribbons. *Nature* **466**, 470-473 (2010).
5.   Han, M.Y., Özyilmaz, B., Zhang, Y. & Kim, P. Energy Band-Gap Engineering of Graphene Nanoribbons. *Physical Review Letters* **98**, 206805 (2007).
6.   Kim, W.Y. & Kim, K.S. Prediction of very large values of magnetoresistance in a graphene nanoribbon device. *Nat Nano* **3**, 408-412 (2008).
7.   Yang, L., Park, C.-H., Son, Y.-W., Cohen, M.L. & Louie, S.G. Quasiparticle Energies and Band Gaps in Graphene Nanoribbons. *Physical Review Letters* **99**, 186801 (2007).
8.   Yan, Q. et al. Intrinsic Current−Voltage Characteristics of Graphene Nanoribbon Transistors and Effect of Edge Doping. *Nano Letters* **7**, 1469-1473 (2007).
9.   Wang, X. et al. Room-Temperature All-Semiconducting Sub-10-nm Graphene Nanoribbon Field-Effect Transistors. *Physical Review Letters* **100**, 206803 (2008).
10.   Bronner, C. et al. Aligning the Band Gap of Graphene Nanoribbons by Monomer Doping. *Angewandte Chemie International Edition* **52**, 4422-4425 (2013).
11.   Cai, J. et al. Graphene nanoribbon heterojunctions. *Nat Nano* **9**, 896-900 (2014).
12.   Martins, T.B., Miwa, R.H., da Silva, A.J.R. & Fazzio, A. Electronic and Transport Properties of Boron-Doped Graphene Nanoribbons. *Physical Review Letters* **98**, 196803 (2007).
13.   Li, Y., Zhou, Z., Shen, P. & Chen, Z. Spin Gapless Semiconductor−Metal−Half-Metal Properties in Nitrogen-Doped Zigzag Graphene Nanoribbons. *ACS Nano* **3**, 1952-1958 (2009).
14.   Terrones, H., Lv, R., Terrones, M. & Dresselhaus, M.S. The role of defects and doping in 2D graphene sheets and 1D nanoribbons. *Reports on Progress in Physics* **75**, 062501 (2012).
15.   Cervantes-Sodi, F., Csányi, G., Piscanec, S. & Ferrari, A.C. Edge-functionalized and substitutionally doped graphene nanoribbons: Electronic and spin properties. *Physical Review B* **77**, 165427 (2008).
16.   Biel, B., Blase, X., Triozon, F. & Roche, S. Anomalous Doping Effects on Charge Transport in Graphene Nanoribbons. *Physical Review Letters* **102**, 096803 (2009).
17.   Nguyen, G.D. et al. Bottom-Up Synthesis of N = 13 Sulfur-Doped Graphene Nanoribbons. *The Journal of Physical Chemistry C* **120**, 2684-2687 (2016).
18.   Chen, Y.-C. et al. Tuning the Band Gap of Graphene Nanoribbons Synthesized from Molecular Precursors. *ACS Nano* **7**, 6123-6128 (2013).
19.   van der Lit, J. et al. Suppression of electron–vibron coupling in graphene nanoribbons contacted via a single atom. **4**, 2023 (2013).
20.   Ruffieux, P. et al. On-surface synthesis of graphene nanoribbons with zigzag edge topology. *Nature* **531**, 489-492 (2016).

21.   Talirz, L. et al. On-Surface Synthesis and Characterization of 9-Atom Wide Armchair Graphene Nanoribbons. *ACS Nano* **11**, 1380-1388 (2017).

22.   Zhang, H. et al. On-Surface Synthesis of Rylene-Type Graphene Nanoribbons. *Journal of the American Chemical Society* **137**, 4022-4025 (2015).

23.   Cloke, R.R. et al. Site-Specific Substitutional Boron Doping of Semiconducting Armchair Graphene Nanoribbons. *Journal of the American Chemical Society* **137**, 8872-8875 (2015).

24.   Kawai, S. et al. Atomically controlled substitutional boron-doping of graphene nanoribbons. **6**, 8098 (2015).

25.   Carbonell-Sanromà, E. et al. Quantum Dots Embedded in Graphene Nanoribbons by Chemical Substitution. *Nano Letters* **17**, 50-56 (2017).

26.   Hybertsen, M.S. & Louie, S.G. Electron correlation in semiconductors and insulators: Band gaps and quasiparticle energies. *Physical Review B* **34**, 5390-5413 (1986).

27.   Koch, M., Ample, F., Joachim, C. & Grill, L. Voltage-dependent conductance of a single graphene nanoribbon. *Nat Nano* **7**, 713-717 (2012).

28.   Chen, Y.-C. et al. Molecular bandgap engineering of bottom-up synthesized graphene nanoribbon heterojunctions. *Nat Nano* **10**, 156-160 (2015).

29.   Ruffieux, P. et al. Electronic Structure of Atomically Precise Graphene Nanoribbons. *ACS Nano* **6**, 6930-6935 (2012).

30.   Ijäs, M. et al. Electronic states in finite graphene nanoribbons: Effect of charging and defects. *Physical Review B* **88**, 075429 (2013).

31.   Horcas, I. et al. WSXM: A software for scanning probe microscopy and a tool for nanotechnology. *Review of Scientific Instruments* **78**, 013705 (2007).

32.   Giannozzi, P. et al. QUANTUM ESPRESSO: a modular and open-source software project for quantum simulations of materials. *Journal of Physics Condensed Matter* **21**, 395502 (2009).

33.   Deslippe, J. et al. BerkeleyGW: A massively parallel computer package for the calculation of the quasiparticle and optical properties of materials and nanostructures. *Computer Physics Communications* **183**, 1269-1289 (2012).
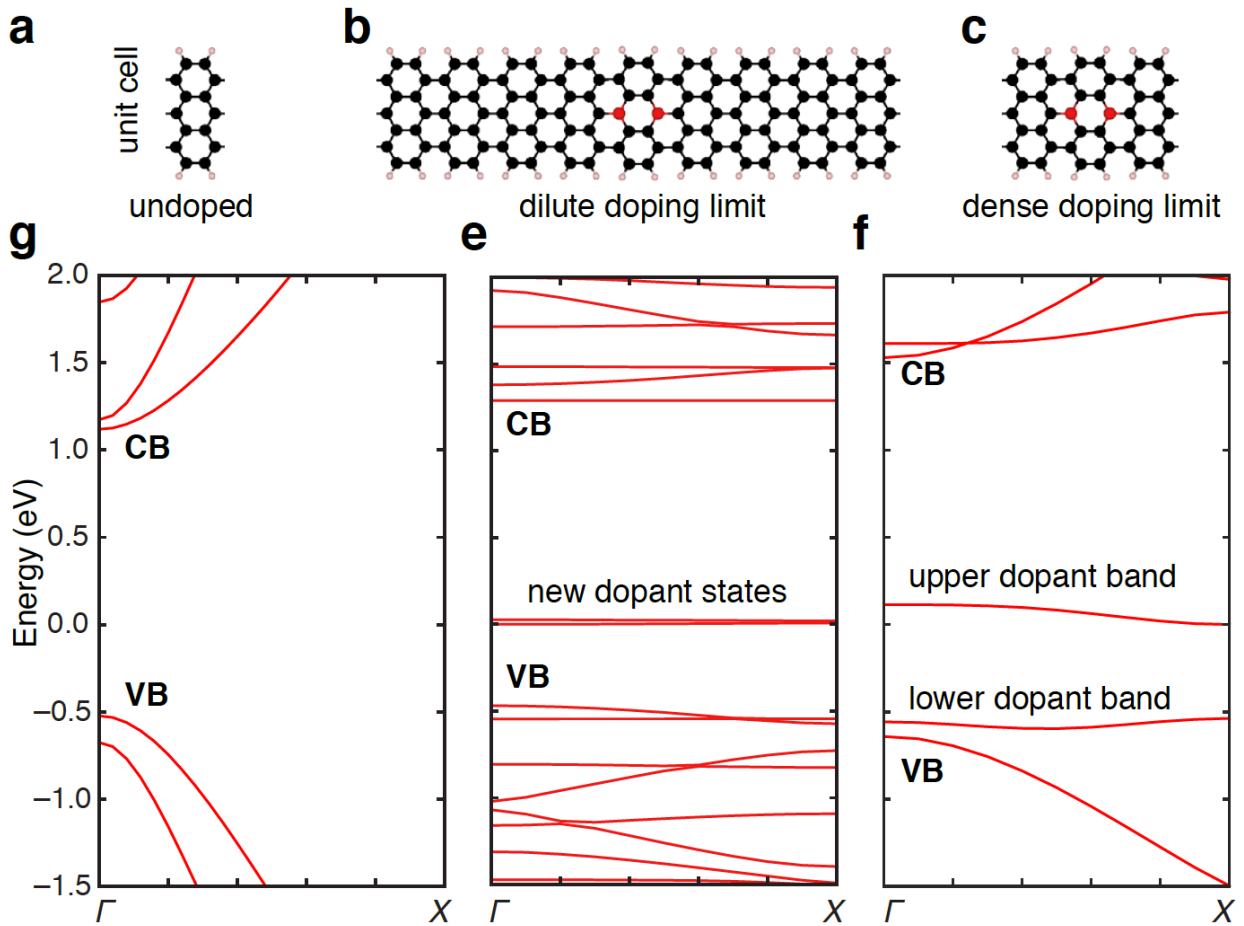
ACKNOWLEDGMENTS

Author contribution

Z.P, C.C., G.D.N., A.A.O, H.T, D.J.R., T.J., C.B., W.C. and M.F.C. performed STM measurements and analyzed STM data. F.Z., T.C. and S.G.L. carried out GNR calculations and interpretation of STM data. R.R.C., T.M. and F.R.F. synthesized the precursor molecules. All authors discussed and wrote the paper.

Figure 1: Band structure evolution of freestanding boron-doped N=7 armchair graphene nanoribbon at different dopant densities. Unit cells of (a) undoped, (b) dilute-doped, and (c) densely doped N=7 GNRs. Red, black, and purple spheres represent boron, carbon, and hydrogen atoms, respectively. (d-f) corresponding band structures calculated by DFT within LDA.
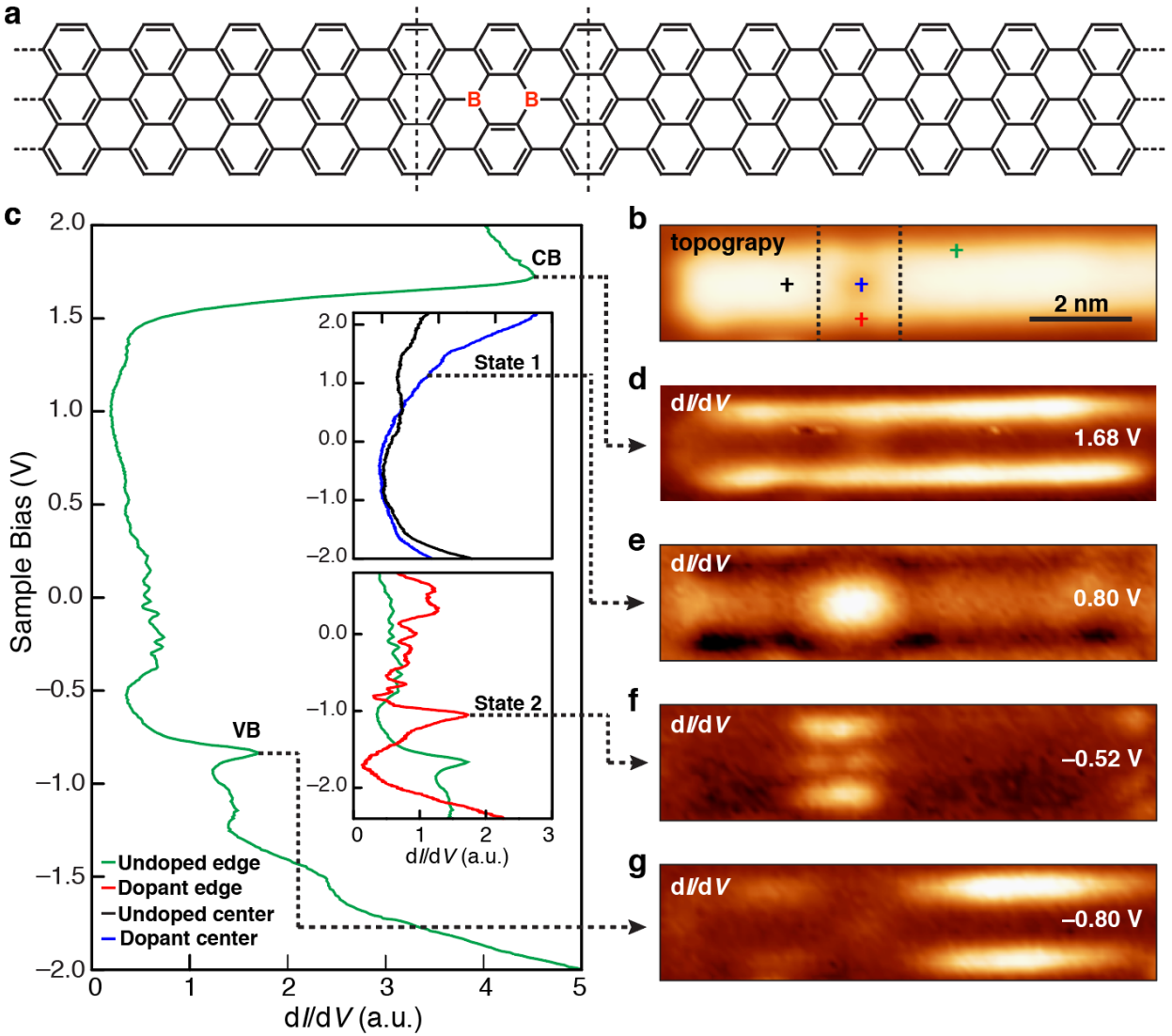
Figure 2: Electronic structure of a dilute boron-doped N=7 AGNR on Au (111). (a) schematic representation of a dilute-doped GNR. (b) STM topographic image of dilute-doped GNR ($V_s = -0.4V$, $I_t = 60pA$). (c) STM dI/dV spectroscopy measurement taken at the edge of an undoped segment of the GNR (green). Top inset shows dI/dV spectroscopy taken at center of boron dimer segment (blue) compared to center of undoped GNR (black). Bottom inset shows dI/dV spectroscopy taken at the edge of boron doped segment (red) compared to edge of undoped GNR

(green). Two new states, dopant State 1 and 2, are observed at –0.5 eV and 0.8 eV respectively.

dI/dV maps of the GNR are shown at energies corresponding to (d) the CB edge (V_s = +1.68V), (e) State 2 (V_s = 0.8 V), (f) State 1 (V_s = –0.5 V), and (g) the VB edge (V_s = –0.8V). T = 7 K for all measurements. (d-g) have the same scale bars.
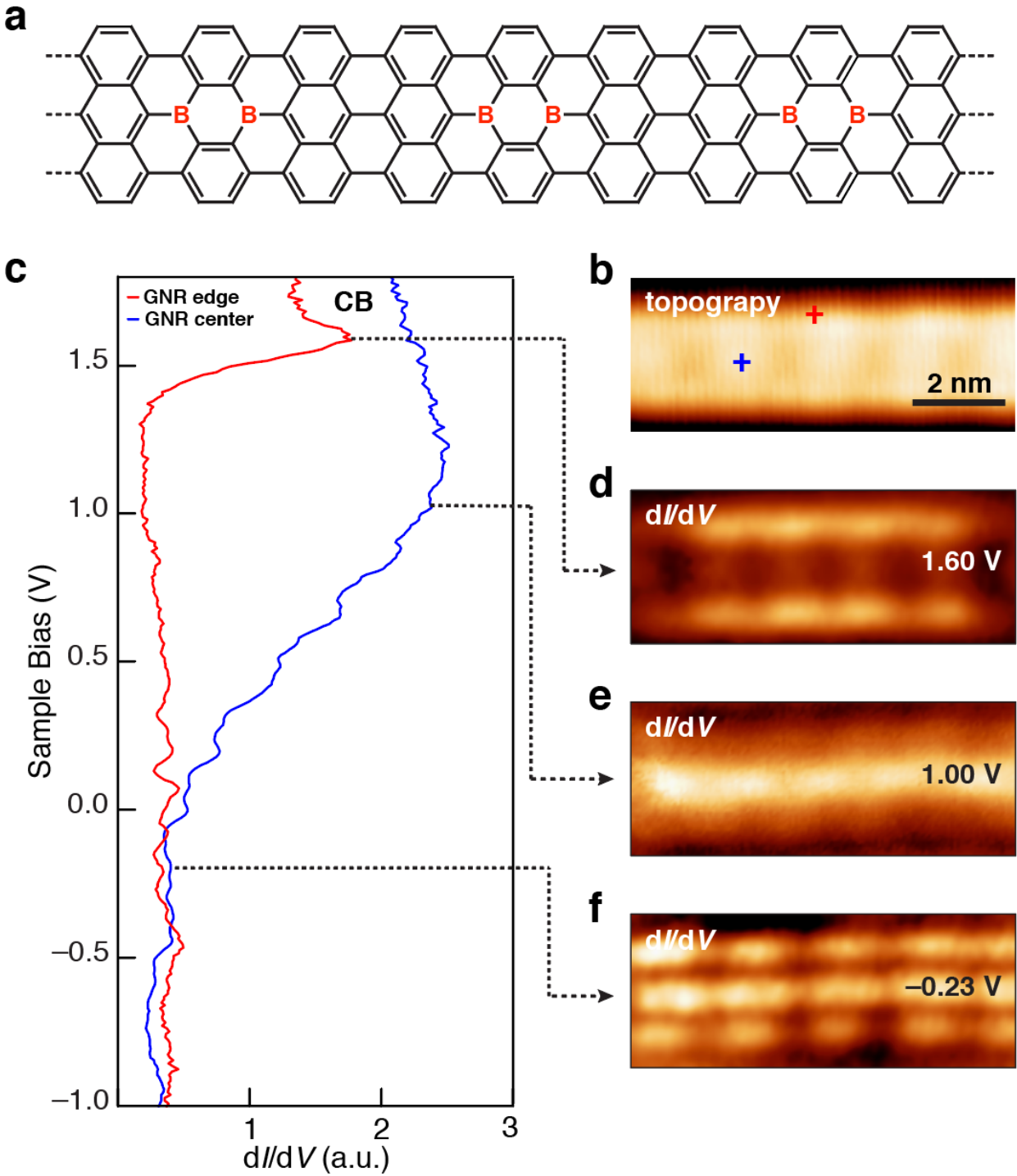
Figure 3: Electronic structure of densely boron-doped N=7 AGNR on Au (111). (a) STM dI/dV spectroscopy measured at the edge and center of a densely-doped GNR. Inset shows locations where spectra were acquired (STM topograph parameters: V_s = 1.60V, I_t = 20pA). (b)Schematic

representation of a densely-doped GNR. (c) dI/dV map taken at $V_s = +1.60$V visualizes state at the CB edge. (d) dI/dV map taken at $V_s = +1.00$V visualizes upper defect band. (e) dI/dV map taken at $V_s = -0.23$V visualizes lower dopant band. $T = 7$ K for all measurements. (c-e) have the same scale bars.
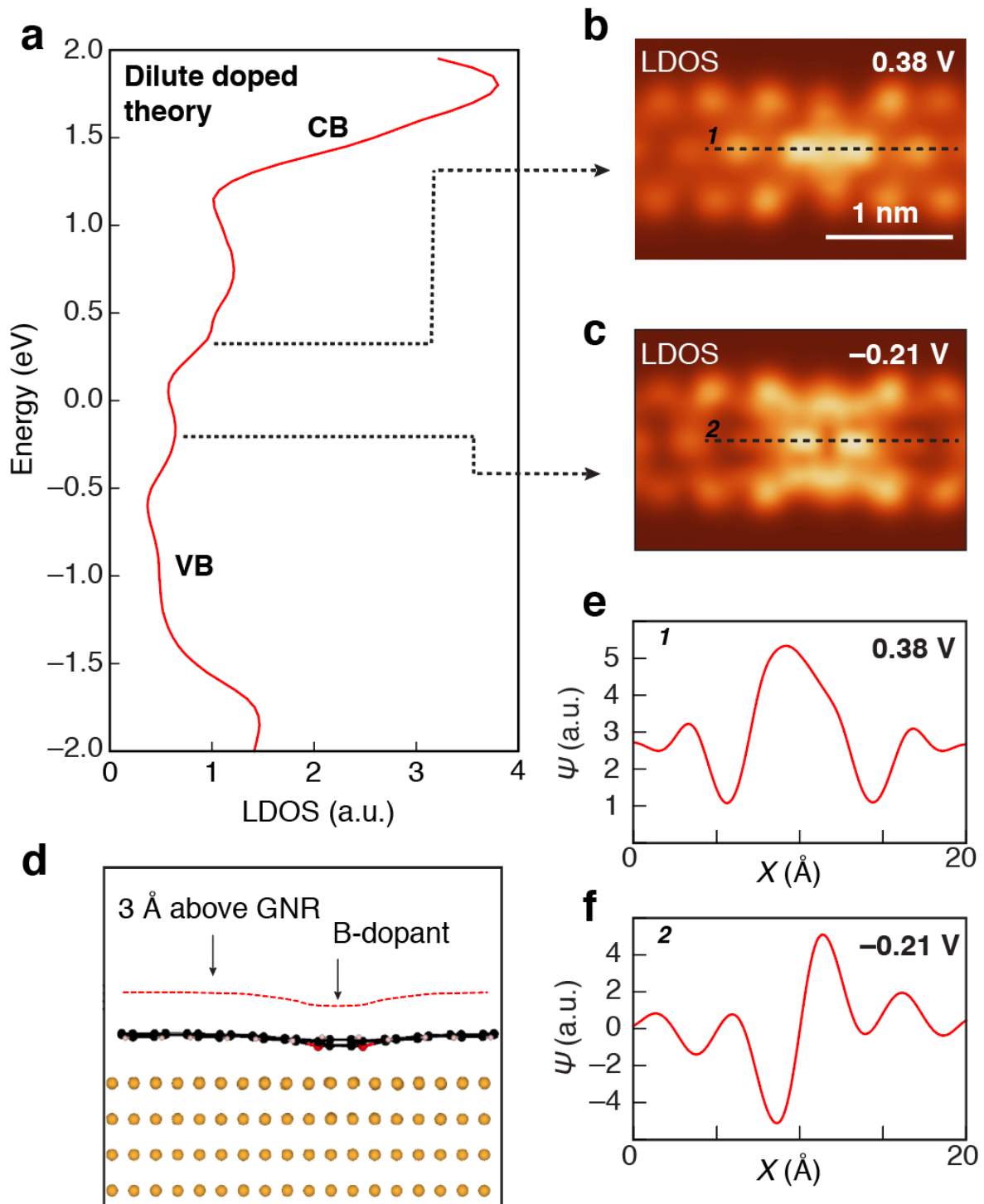
Figure 4: DFT-LDA calculation of dilute-doped N=7 GNR on Au (111) substrate. (a) Calculated

LDOS 3Å above boron doped segment shows dopant States 1 and 2 (theoretical LDOS is

broadened by a 150meV wide Gaussian function). Calculated density map is shown for (b) 0.38 eV (integrated over a 0.05 eV energy window) and (c) –0.21 eV (integrated over a 0.05 eV energy window). (d) Side-view of the supercell structure of the relaxed dilute-doped GNR that includes 4 layers of Au (111). Red dashed line shows the plane where the LDOS and density maps are calculated. Calculated wavefunctions along an axial line (black dashed) 3Å above the GNR extending through the boron doped segment at the energy of (e) State 2 and (f) State 1. (b) and (c) have the same color bars.